Title

Silencing the Snail-dependent RNA splice regulator ESRP1 drives malignant transformation of human pulmonary epithelial cells

Journal

Cancer Research, 78(8)

ISSN

0008-5472

Authors

Walser, Tonya C

Jing, Zhe

Tran, Linh M

et al.

Publication Date

2018-04-15

DOI

10.1158/0008-5472.can-17-0315

Peer reviewed

HHS Public Access

Author manuscript

Cancer Res. Author manuscript; available in PMC 2019 April 15.

Published in final edited form as:

Cancer Res. 2018 April 15; 78(8): 1986–1999. doi:10.1158/0008-5472.CAN-17-0315.

Silencing the Snail-dependent RNA splice regulator ESRP1 drives malignant transformation of human pulmonary epithelial cells

Tonya C. Walser[1,2,5,*], **Zhe Jing**[1,2,5], **Linh M. Tran**[1,2,5], **Ying Q. Lin**[1,2,5], **Natalie Yakobian**[1,2,5], **Gerald Wang**[1,2,5], **Kostyantyn Krysan**[1,2,5], **Li X. Zhu**[1,2,5,6], **Sherven Sharma**[1,2,5,6], **Mi-Heon Lee**[7], **John A. Belperio**[1,2,5], **Aik T. Ooi**[5,8,9], **Brigitte N. Gomperts**[5,8,9], **Jerry W. Shay**[10], **Jill E. Larsen**[11], **John D. Minna**[12], **Long-sheng Hong**[3], **Michael C. Fishbein**[3], and **Steven M. Dubinett**[1,2,3,4,5,6,*]

[1]Division of Pulmonary and Critical Care Medicine, David Geffen School of Medicine at UCLA, Los Angeles, CA.

[2]Department of Medicine, David Geffen School of Medicine at UCLA, Los Angeles, CA.

[3]Department of Pathology and Laboratory Medicine, David Geffen School of Medicine at UCLA, Los Angeles, CA.

[4]Department of Molecular and Medical Pharmacology, David Geffen School of Medicine at UCLA, Los Angeles, CA.

[5]Lung Cancer Research Program, Jonsson Comprehensive Cancer Center at UCLA, Los Angeles, CA.

[6]VA Greater Los Angeles Health Care System, Los Angeles, CA.

[7]Department of Surgery, David Geffen School of Medicine at UCLA, Los Angeles, CA.

[8]Department of Pediatrics, David Geffen School of Medicine at UCLA, Los Angeles, CA.

[9]Mattel Children's Hospital at UCLA, Los Angeles, CA.

[10]Department of Cell Biology, The University of Texas Southwestern Medical Center, Dallas, TX.

[11]QIMR Berghofer Medical Research Institute, Brisbane, Australia.

[12]Hamon Center for Therapeutic Oncology Research, The University of Texas Southwestern Medical Center, Dallas, TX.

Abstract

[*]**Corresponding Author:** To whom correspondence should be addressed: Tonya C. Walser and Steven M. Dubinett, Division of Pulmonary and Critical Care Medicine, David Geffen School of Medicine at UCLA, 37-131 Center for Health Sciences, 10833 Le Conte Avenue, Los Angeles, CA 90095. Phone: 310-267-2725; Fax: 310-267-2829; twalser@mednet.ucla.edu and sdubinett@mednet.ucla.edu.

Conflict of Interest Disclosure: At the time of publication, Dr. Ooi is a paid employee of Fluidigm Corporation, and Dr. Gomperts is an uncompensated consultant at InSpira.

Data and Material Availability: HBEC and HSAEC lines were obtained through an MTA with UTSW. NSG mice were obtained through an MTA with Jackson Laboratories. Gene and miRNA expression profiling data are available at www.ncbi.nlm.nih.gov/geo (accession number GSE108137).

Epithelial-to-mesenchymal transition (EMT) is organized in cancer cells by a set of key transcription factors, but the significance of this process is still debated including in non-small cell lung cancer (NSCLC). Here we report increased expression of the EMT-inducing transcription factor Snail in premalignant pulmonary lesions, relative to histologically normal pulmonary epithelium. In immortalized human pulmonary epithelial cells and isogenic derivatives, we documented Snail-dependent anchorage-independent growth in vitro and primary tumor growth and metastatic behavior in vivo. Snail-mediated transformation relied upon silencing of the tumor suppressive RNA splicing regulatory protein ESRP1. In clinical specimens of NSCLC, ESRP1 loss was documented in Snail-expressing premalignant pulmonary lesions. Mechanistic investigations showed that Snail drives malignant progression in an ALDH+CD44+CD24- pulmonary stem cell subset in which ESRP1 and stemness-repressing microRNAs are inhibited. Collectively, our results show how ESRP1 loss is a critical event in lung carcinogenesis, and they identify new candidate directions for targeted therapy of NSCLC.

Keywords

cancer interception; lung carcinogenesis; Snail; epithelial-to-mesenchymal transition (EMT); epithelial splicing regulatory protein 1 (ESRP1)

Introduction

Lung cancer is the leading cause of cancer mortality worldwide. Defining the molecular abnormalities that precipitate lung cancer initiation will facilitate the development of cancer interception strategies that improve outcomes for lung cancer patients (1).

Weinberg and colleagues were the first to report that induction of EMT in immortalized murine mammary epithelial cells leads to acquisition of mesenchymal traits, expression of stem cell markers, and ultimately malignant transformation, in part via expansion of a $CD44^{+}CD24^{-}$ stem cell subset (2). Several EMT-inducing transcription factors, including Snail, have since been found to bind to E-boxes in the *ESRP1* promoter causing repression of the splicing regulator, promotion of EMT, and induction of tumorigenesis in other model systems (3–5). Clearly defined roles for Snail and ESRP1 in human lung cancer initiation have not yet been reported.

The objective of this study was to provide evidence of Snail expression in lung premalignancy *in situ* and to document the protracted Snail-dependent carcinogenesis process *in vitro* and *in vivo*. Identification of a clinically relevant mechanism for Snail-driven transformation of pulmonary epithelial cells was paramount, as was providing evidence for/against the proposed mechanism in Snail-expressing clinical specimens. The human bronchial epithelial cell (HBEC) model was utilized to isogenically assess the contribution of Snail to malignant transformation. Gene expression profiling of Snail-expressing HBECs revealed a marked and consistent suppression of ESRP1. Evaluation of ESRP1 tumor suppressor activity in genetic reversal studies identified ESRP1 silencing as a novel mechanism underlying Snail-driven stem cell expansion and pulmonary epithelial cell transformation. Observation of ESRP1 loss concomitant with Snail and stem cell marker expression in human pulmonary premalignancy suggests that the Snail-ESRP1-cancer axis is

operative during lung carcinogenesis *in situ*. Identification of Snail-dependent carcinogenesis signatures from genetically-defined HBEC-Snail cells provides early insight into potential targets for disruption of the pulmonary epithelium-to-lung cancer continuum, now termed lung cancer "interception" (1).

Materials and Methods

Clinical specimens

All clinical samples were obtained with written informed consent from patients. All studies were approved in advance by the UCLA institutional review board, and they were performed in accordance with the Declaration of Helsinki. Pulmonary premalignant lesions were obtained from surgically resected human lung tissues archived in the UCLA Lung Cancer SPORE Tissue Repository (IRB #10-001096). Eleven squamous metaplasia (SM) premalignant lesions were found proximal to squamous cell carcinoma (SCC) tumors, and twelve atypical adenomatous hyperplasia (AAH) premalignant lesions were found proximal to adenocarcinoma (ADC) tumors. Twenty-seven histologically normal-appearing large airways (LAs; bronchi > segmental bronchus) served as controls for the SM lesions, and twenty-eight histologically normal-appearing small airways (SAs; alveoli < terminal bronchiole) served as controls for the AAH lesions. Five unrelated normal (Nor) lung tissues derived from non-cancer trauma cases (IRB #11-001051) served as additional negative controls. Other abnormalities found in the airways of patients with lung cancer or in the explanted lungs of patients with chronic obstructive pulmonary disease (COPD) (IRB #13-000462) were available for immunostaining in smaller numbers (n=12); regions of interest included airway defects (n=2), fields of hyperplasia (n=7), adenocarcinoma *in situ* (AIS) (n=5), along with any instances of SM (n=6) or AAH (n=6) in the COPD biospecimens.

Cell lines

Immortalized HBEC lines were established by introducing cyclin-dependent kinase 4 and human telomerase reverse transcriptase into normal HBECs isolated from the large airways of patients (6,7). Five parental cell lines derived from five patients were utilized here, including HBEC2, HBEC3, HBEC4, HBEC7, and HBEC11. As previously described (6), HBEC3 was subsequently engineered to recapitulate the proto-oncogene activation (KRAS and EGFR) and tumor suppressor silencing (P53) that often characterizes the airways of those who smoke and are at-risk for lung cancer development. HSAEC21, an immortalized human small airway epithelial cell (HSAEC) line, was also investigated in select experiments. All cell lines were routinely tested and confirmed to be free of Mycoplasma using the MycoAlert Mycoplasma Detection Kit (Lonza Walkersville). Cell lines were authenticated in the UCLA Genotyping and Sequencing Core utilizing Promega's DNA IQ System and Powerplex 1.2 system, and all cells were used within 10 passages of genotyping. All HBEC and derivative cell lines were cultured in Keratinocyte Serum-Free Medium (KSFM) supplemented with 30 μg/mL Bovine Pituitary Extract and 0.2 ng/mL recombinant Epidermal Growth Factor 1–53 (all Life Technologies), henceforth called KSFM complete medium. Cell cultures were grown at 5% CO_2 and 37° C.

Murine model of lung carcinogenesis

Pathogen-free NOD.Cg-*Prkdc*^{scid} *Il2rg*^{tm1Wjl}/SzJ (NOD SCID Gamma or NSG; Jackson Labs strain #005557) mice, 6–12 weeks of age, were maintained at the West Los Angeles Veterans' Administration Animal Research Vivarium or the UCLA Division of Laboratory Animal Management Biocontainment Facility. All studies were approved by the appropriate institution's animal studies review board (VA IACUC and UCLA ARC #2011-084). Cells (5×10^6) were implanted subcutaneously (SC) into the left flank of each mouse, and tumor growth was assessed three times per week. Two bisecting diameters of each tumor were measured with calipers, and tumor volume was calculated using the formula $0.4x ab^2$, where *a* represents the longer diameter and *b* the shorter diameter. At the time of harvest, primary tumors were formalin-fixed paraffin-embedded (FFPE) and assessed for primary tumor histology and the presence of metastatic disease. For select experiments, the primary tumor was dissociated and inoculated into new NSG mice to assess the impact of *in vivo* passaging on tumor-take rate and the lag phase proceeding initial tumor palpation. H&E staining and select immunostaining were performed as previously described using the antibodies and conditions summarized in Table S1.

Statistical analysis

Samples were plated and run in triplicate, and all experiments were performed at least three times, unless otherwise indicated. Results from one representative experiment or image are shown. Probability values were calculated using the two-tailed non-paired Student's *t*-test for count-based data. ANOVA models were utilized where multiple pairwise comparisons were made, unless otherwise indicated. Data are reported as significant as follows: * if $p \leq 0.05$, ** if $p \leq 0.001$, and *** if $p \leq 0.0001$.

Results

Snail expression is observed in human pulmonary premalignant lesions

To determine if Snail is expressed *in situ* during the early stages of lung cancer development, SCC and ADC premalignant lesions were immunostained for Snail. Isotype, negative, and positive controls stained appropriately (Fig 1A i–iii). Snail staining of tumor-adjacent histologically normal-appearing LAs (Fig 1A iv–vi) and SAs (Fig 1A vii–ix) was faint to negative. In contrast, premalignant epithelial cells comprising SM (Fig 1A x–xii) and AAH (Fig 1A xiii–xv) lesions were strikingly positive for nuclear Snail staining. Snail staining of premalignant epithelial cells was frequently characterized by nearby foci of inflammation (*e.g.*, Fig 1A xi). By scoring the immunostaining of SM lesions (n = 11), AAH lesions (n = 12), tumor-adjacent histologically normal airways (n = 23), and normal (Nor) lung tissues (n = 5), we determined that Snail expression is significantly elevated in human pulmonary premalignancy (Fig 1B). The intensity×positivity (IxP) score of SM lesions was 5.6, higher than both of its controls (LA = 3.3 and Nor = 1.0; p = 0.1446 and p < 0.0001, respectively). The IxP score of AAH lesions was 3.6, higher than both of its controls (SA = 0.3 and Nor = 0.2; p = 0.0592 and p = 0.0016, respectively).

These findings were reproducible utilizing two Snail antibodies stringently validated for sensitivity and specificity. This assessment included isotype and blocking antibodies,

negative and positive control clinical specimens, as well as HBEC-Vector and -Snail 3D culture negative and positive controls (Fig S1A and S1B). An investigation of Snail in areas of airway injury revealed robust nuclear Snail expression in these regions as well. Specifically, airway defects and airways in 1) regions of extensive lung destruction, 2) fields of hyperplasia, and 3) premalignant lesions observed in the lung explants of COPD patients without lung cancer were all robustly positive for Snail expression relative to the appropriate controls (Fig S1C i–vi). AIS lesions, hypothesized to occur temporally in the lung carcinogenesis continuum between AAH lesions and minimally invasive adenocarcinoma (MIA) and ADC tumors, were also strikingly positive in all observed cases (Fig S1C vii–viii).

We previously reported a reciprocal relationship between Snail and E-cadherin expression in established SCC and ADC tumors (8). However, a panel of SM (n = 4) and AAH (n = 5) lesions, as well as two distinctive airway defects, double-stained for Snail and E-cadherin revealed the presence of E-cadherin epithelial cell surface staining despite intense Snail nuclear staining in the same cells (Fig S1D). These data suggest that the role of Snail in pulmonary premalignancy *in situ* may be independent of E-cadherin loss.

Snail drives EMT in an HBEC-based model of human lung premalignancy

We ectopically expressed Snail in five HBEC lines derived from basal cells isolated from the large airways of five human subjects. Regardless of the level of Snail expression, E-cadherin expression was maintained in the HBEC-Snail cells (Fig 1C) (Fig S2A), in agreement with the above observations of premalignant epithelial cells *in situ*. We extended the examination of Snail to an additional cell line, HSAEC21, derived from type II pneumocytes isolated from the small airways of a human subject. Forced expression of Snail in HSAEC21 completely repressed E-cadherin (Fig S2A), more typical of Snail's impact in lung cancer cells (8). Thus, a role for E-cadherin repression in Snail-dependent events in the small airway cannot be ruled out. Finally, Snail was expressed in a panel of oncogene-modified HBECs shown to accurately recapitulate the airways and premalignant lesions of patients at-risk for lung cancer development (7). Whether the underlying lung-relevant mutation was *TP53*, *KRAS*, or *EGFR*-related, a similar pattern of Snail and E-cadherin expression was observed; Snail was expressed, and E-cadherin was either not impacted or impacted only modestly in the oncogene-modified HBEC3 cells (Fig 1D) (Fig S2B).

A diverse panel of epithelial and mesenchymal molecular markers was surveyed to determine if Snail expression by pulmonary epithelial cells drives the EMT program, as we had previously observed in established lung cancer cells (8). Snail expression by HBECs induces EMT, as numerous prototypical pulmonary epithelial markers are down-regulated and several mesenchymal markers are up-regulated (Fig 1E). Morphologically, HBEC-Snail cells assume an elongated spindle shape that is indicative of EMT and distinct from the round cobblestone morphology of the control cells (Fig 1F). These findings indicate that Snail expression induces normal non-mutated cells of the bronchial epithelium to undergo alterations consistent with EMT, despite its modest impact on E-cadherin.

Genomic and proteomic profiling reveal Snail-driven cancer-associated signaling nodes operative during pulmonary premalignancy

To identify signaling networks activated by isogenic Snail expression in pulmonary epithelial cells, we characterized gene, miRNA, and protein expression in the genetically-defined HBEC-Snail cells utilizing high-throughput platforms. Bioinformatic analysis of the HBEC-Snail gene expression signature revealed significant overlap and appropriate directionality relative to The Cancer Genome Atlas (TCGA) lung SCC and ADC clinical datasets (Fig 2A i–ii). Gene set enrichment analysis (GSEA) was utilized to identify gene sets significantly enriched in the HBEC expression data. A correlation was observed between HBEC-Snail gene expression signatures and gene sets characterizing: 1) poorer survival in lung cancer, 2) increased metastasis in melanoma, 3) enhanced mesenchymal histology in breast cancer, as well as 4) embryonic stem cell, 5) undifferentiated cancer, and 6) anti-proliferative (pro-motility) signaling events observed in cancer models (Fig S3A). Consistent with our previous finding of decreased survival for lung ADC patients with high tumor Snail expression (8), our current analysis of TCGA data from 425 SCC tumors revealed significantly decreased survival for patients with tumors that exhibited the highest levels of Snail mRNA expression (Fig 2B). Additional network analyses allowed the integration of the mRNA and miRNA data, thus facilitating ranking of the potentially important miRNA candidates based on their impact on expression of target genes also influenced by Snail in the mRNA data (Fig 2C) (Fig S3B). Both the miRNA and target genes are predominantly members of EMT, invasion, stemness, and apoptosis signaling nodes, as well as oncogene and tumor suppressor gene pathways. Fifty specific cancer-related proteins were also queried. By Luminex immunoassay, numerous differentially expressed proteins were observed with secretion patterns indicative of Snail-mediated inflammation (Fig 2D), invasion (Fig 2E), and angiogenesis (Fig 2F–H). A subset of these Luminex-based findings was also investigated in protein-specific ELISA assays, where the impact of Snail on CXCL8 and CXCL5, for example, was augmented when the HBECs were assessed in 3D culture compared to 2D culture (Fig S3C–D).

Snail drives key malignant phenotypes in 2D and 3D models of lung carcinogenesis

In a 3D spheroid culture model, HBEC-Vector cells form compact spheroidal colonies, whereas HBEC-Snail cells form stellate aggregates with invasive projections (Fig 3A). The spindle-shaped morphology of the clusters suggests that Snail expression drives both EMT and invasion in this model, consistent with our previous findings in 2D (9). In a 3D organotypic air-liquid interface (ALI) model of premalignancy, HBEC-Vector cells differentiate, forming a well-organized epithelial cell layer atop the modified basement membrane (BM) (Fig 3B). In contrast, the HBEC-Snail epithelial cell layer is poorly differentiated, disorganized, discohesive, and exhibits invasive behavior, as the epithelial cells invade beneath the BM. Immunostaining of E-cadherin is intense in the HBEC-Vector epithelial layer, but nearly absent in the HBEC-Snail cells grown in 3D ALI culture (Fig 3B); isotype controls were negative (Fig S4A).

In the same 3D ALI model, staining with markers for basal or progenitor cells of the lung epithelium, Ck14 and p63, is appropriately restricted to the basal epithelial cell layer in HBEC-Vector cultures (Fig 3C). In contrast, HBEC-Snail cultures are uniformly positive for

the markers regardless of the location of the cells within the epithelium and underlying mucosa, suggesting loss of polarity and expansion of the progenitor cell population. Epithelial cells positive for ALDH1/2 and CD44 are also more numerous and less restricted to the basal layer in the HBEC-Snail cultures compared to HBEC-Vector cultures (Fig 3C and Fig S4B, respectively). Observation of increased proliferation in the HBEC-Snail 3D cultures, indicated by Ki67 staining, supports the concept of Snail-driven basal cell expansion within the HBEC lung progenitor cells (Fig 3C). Loss of P53 and KRAS activation in the same HBEC cells does not promote a similar expansion of the stem-like cells (Fig S4B), confirming that expansion of this progenitor cell population is not a general response to genetic insult. Fluorescent immunostaining with image overlay confirms that Snail and ALDH1/2 expression are resident within the same epithelial cells, shown in **yellow** following **red** (ALDH1/2) and **green** (Snail) image merge (Fig S4C). These findings indicate that Snail expression drives EMT in human pulmonary epithelial cells and initiates a program of invasion and basal cell population expansion.

Flow cytometry was performed to determine the percentage of cells in the HBEC progenitor population driven toward a stem-like state by Snail expression and initiation of the EMT signaling program. The $ALDH^+$ stem cell population is expanded by ~9-fold in HBEC-Snail compared to HBEC-Vector (Fig 4A), and the $CD44^+CD24^-$ cancer stem cell phenotype is expanded by ~14-fold (Fig 4B). Apoptosis-resistance is another functional characteristic ascribed to cells with enhanced “stemness.” Compared to HBEC-Vector cells, HBEC-Snail cells are ~12-fold more resistant to apoptosis induced by detachment and serum-starvation (Fig 4C) or staurosporine treatment (Fig 4D), as measured by Annexin-V staining and flow cytometry analysis. Finally, Western blot analysis confirmed Snail-dependent up-regulation of the proto-oncogenes RAB25 (Fig 4E) and down-regulation of several putative tumor suppressors, including EMP3 and GAS1 (Fig 4E), as well as ESRP1 (Fig 4F). Together, these findings in human epithelial cells are consistent with previous reports of murine basal cells functioning as multipotential pulmonary progenitor cells capable of malignant transformation (10).

Snail-driven malignant transformation is augmented by driver mutations and is dependent on acquisition of stem-like traits in vitro

In both HBEC3 and HBEC4 cells, Snail expression drives robust anchorage-independent growth (AIG) of histologically normal cells of the bronchial epithelium (Fig 5A). Quantitation of the assay reveals statistically significant Snail-driven AIG of the epithelial cells (H3 FC = 3.2 and H4 FC = 1.8, both $p < 0.0001$) that is similar to the intrinsic AIG growth rate of A549 tumor cells. As shown in Figure S5A, HBEC3- and HBEC4-Snail cells show inhibited proliferation compared to their Vector control counterparts (H3 72 hr FC = 1.6 and H4 72 hr FC = 1.7, both $p < 0.0001$), indicating that Snail does not confer a simple proliferative advantage to HBECs, rather they are truly transformed. The importance of Snail expression in transformation was also demonstrated in HBEC2 (Snail = 2.5 Units or U vs Vector = 1.3U, $p = 0.0237$) and HBEC11 (Snail = 1.9U vs Vector = 1.4U, $p = 0.1104$) cells (Fig S5B), as well as in distal airway HSAEC21 cells (Fig S5C).

Snail also drives the transformation of HBEC3-mutant-Snail cells with either activated *KRAS* or *EGFR* or silenced *TP53*, although the most pronounced results are observed in *P53/KRAS* double-mutant cells (Fig S5D–E). Molecular and functional characterization of a secondary panel of cells yielded the same results, as shown in representative Western blot and AIG results (Fig S5F). Prior to evaluating the oncogene-modified HBEC-Snail cells in mice, the minimum number of mutational events required to yield the largest AIG colonies was determined *in vitro*. As shown in Figure S5D, the contribution of KRAS mutation (HBEC3mutantKRAS-Snail) to the transformation potential of Snail appears to be negligible in the *in vitro* assay. Conversely, P53 loss (HBEC3mutantP53-Snail) yields AIG colonies equivalent to the most aggressive HBEC3mutantP53/KRAS-Snail AIG colonies observed (Fig S5D and Fig 5B), consistent with the observations of others in murine model systems (11).

To better characterize the cell type sensitive to Snail induction of AIG, flow cytometry sorting was utilized to isolate the stem cell subsets shown above to be responsive to Snail expression. The critical requirement for ALDH1/2 for Snail-driven AIG of HBEC4 cells was identified by first seeding $ALDH^+$ and $ALDH^-$ cells in separate AIG assays (Fig S6A). Next, the $ALDH^+$ Snail cells were separated into the $CD44^+CD24^-$ cancer stem cell subpopulation and a control population ($CD44^+CD24^+$ cells) (Fig S6B). When plated in the AIG assay, the $ALDH^+CD44^+CD24^-$ cancer stem cell subset of HBEC4-Snail cells yielded large AIG colonies (5.9U) that were equivalent to the A549 control cells (5.5U); lack of ALDH, CD44, and/or presence of CD24 abrogated the capacity of Snail cells to form colonies, rendering them equivalent to HBEC4-Vector cells (1.7U) in terms of their AIG capacity ($p < 0.0001$) (Fig 5C). The $ALDH^+CD44^+CD24^-$ phenotype, observed at low frequency in HBEC-Vector cells, was insufficient to drive transformation of the HBECs absent Snail expression (1.4U) (Fig 5C). The observation that Snail-dependent AIG requires ALDH activity, CD44 expression, and CD24 loss, in combination, was consistent in HBEC3-Snail (4.6U vs 1.8U, $p < 0.0001$) (Fig S6C) cells. Furthermore, suppression of key microRNAs (miRs) that may underlie the Snail-dependent expansion of this cancer stem cell population was identified (12,13). Stemness-repressing miR-200c, miR-203, and miR183 were all inhibited in HBEC3-, HBEC4-, and HBEC3mutP53/KRAS-Snail cells relative to -Vector cells as measured by qRT-PCR (Fig S6D–F), and they were completely repressed in the flow-sorted $Snail^+ALDH^+CD44^+CD24^-$ cancer stem cell population relative to its controls (Fig S6G–I).

Snail drives malignant transformation, tumor growth, and metastasis of HBECs in vivo

HBEC3-Snail and HBEC3mutantP53-Snail cells did not yield orthotopic lung tumors, whereas HBEC3mutantP53/KRAS-Snail cells injected SC into NSG mice are transformed and give rise to large primary tumors with predominantly SCC histology (Fig 6A *left*). Overall, HBEC3mutantP53/KRAS-Snail cells formed primary lung tumors in 13/35 (37%) mice injected, while 0/22 (0%) mice injected with HBEC3mutantP53/KRAS-Vector cells developed primary lung tumors (summarized in Table S2). The time to tumor palpation ranged from 54 to 84 days (Fig S7A *left*). All mice sacrificed after their Snail-expressing tumors reached $1000mm^3$ in volume were noted to harbor lung metastases (Fig 6A *right*). The time to metastatic disease after the primary tumor became palpable ranged from 22 to

32 days. When Snail primary tumor cells were isolated and re-inoculated into new NSG mice, 4/4 (100%) of the $1x10^6$ cell transplants grew progressively after a short lag phase (15 days on average to palpation) (Fig S7A *right*). Collectively, these data indicate that Snail drives at-risk epithelial cells bearing lung-relevant driver mutations to both transformation and metastatic behavior *in vivo*.

The human primary tumors and lung metastases xenografts were next examined for those mediators found to be critical for Snail-dependent lung cancer-initiating capacity *in vitro*, including Snail, ALDH1/2, and CD44. By immunohistochemical (IHC) evaluation, the transformed HBEC3mP53/KRAS-Snail cells retained each of these critical markers both within the primary tumor and lung metastases (Fig 6B); isotype controls were negative (Fig S4A). To further define the precise isoform of ALDH that may be relevant during lung cancer initiation and progression, the primary tumors and lung metastases were immunostained for ALDH1A3 and ALDH3A1, the two isoforms most frequently implicated in lung cancer (14,15). Both 1A3 and 3A1 isoforms are expressed at high levels in the xenografted primary tumors as well as in the pulmonary metastases (Fig S7B). To determine the potential clinical relevance of this finding in the murine model, 1A3 and 3A1 isoforms were examined in human lung cancers and premalignant lesions. The staining patterns observed in these cases (Fig 6C) suggest that the precise ALDH isoform of the lung progenitor cell that is responsive to Snail transformation may be lung compartment-dependent, consistent with the concept that the source of large and small airway stem cells differ (10,16). Finally, PCR evaluation of the xenografted HBEC3mP53/KRAS-Snail tumors revealed marked suppression of miR-203 relative to all available controls, consistent with our observations *in vitro* (Fig S7C).

Snail-dependent ESRP1 silencing drives human pulmonary epithelial cell transformation

Gene array analysis revealed that ESRP1 expression in HBEC-Snail cells is decreased by 38.8-fold ($p = 0.0076$) compared to levels in HBEC-Vector cells. Because ESRP1 has been implicated in the suppression of EMT, motility, stemness, and anoikis resistance (17,18), the contribution of ESRP1 silencing to key Snail-driven malignant phenotypes was investigated *in vitro* and *in vivo*. Confirming the array results, ESRP1 RNA transcript levels were significantly diminished in HBEC3-, HBEC4-, and HBEC3mutP53/KRAS-Snail cells relative to their vector control counterparts (Fig 7A). Additional cell lines, each from a different human subject, were also examined (Fig S8A). Consistent with these gene expression results, ESRP1 protein is inhibited in HBEC2-, HBEC3-, HBEC4-, HBEC3mutP53-, and HBEC3mutP53/KRAS-Snail cells relative to their vector controls (Fig 4F and 7B); there was no baseline expression of ESRP1 in HBEC11 (Fig 8B).

To determine if ESRP1 loss is required for Snail-dependent AIG, transient expression of ESRP1 was performed in HBEC3- and HBEC3mutP53/KRAS-Vector and -Snail cells (Fig 7C). When these cells with ectopic expression of ESRP1 were plated in the AIG tumorigenicity assay, Snail-dependent AIG was abrogated in both the HBEC3- (Fig 7D) and HBEC3mutP53/KRAS-Snail (Fig 7E) cell lines. To allow assessment of Snail-dependent ESRP1 silencing as a mechanism of HBEC malignant transformation *in vivo*, HBEC3- and HBEC3mutP53/KRAS-Snail cell lines with stable expression of ESRP1 were also generated

(Fig 7F and 7G, **respectively**). Snail-dependent AIG was again abrogated in both the HBEC3- (Fig 7H) and HBEC3mutP53/KRAS-Snail (Fig 7I) cell lines. These results were confirmed using new HBEC-Snail+ESRP1 cells engineered via two different molecular approaches (Fig 7J).

To determine if ESRP1 loss alone is oncogenic, siRNAs were utilized to transiently knock-down *ESRP1* in a panel of HBEC-Vector cells, including HBEC3-, HBEC4-, and HBEC3mutP53/KRAS-Vector. ESRP1 is significantly inhibited in the ESRP1 siRNA group and unaffected in the scramble control, transfection reagent control, and untreated groups (Fig S8B), and it was determined that the transient knockdown persists throughout the course of the assay (Fig S8C). When plated in the *in vitro* tumorigenicity assay, ESRP1 silencing alone was not sufficient to drive AIG of the HBEC-Vector cells (Fig S8D). Collectively, these data suggest that ESRP1 loss is required for Snail-driven transformation, but it is not alone sufficient for the induction of AIG in HBECs.

To determine if ESRP1 repression is required for Snail-driven transformation of HBECs *in vivo,* HBEC3mutP53/KRAS-Snail cells with stable expression of ESRP1 and controls were injected SC into NSG mice. Overall, the Snail-expressing control cells formed tumors in 5/9 (56%) mice injected, while 0/8 mice injected with the HBEC-Snail+ESRP1 cells formed tumors after six months (summarized in Table S2). Times to palpation and metastasis were similar to those observed with the parent Snail-expressing cells. These data indicate that ESRP1 silencing is required for Snail-dependent malignant transformation of HBECs *in vivo*.

Given the importance of ESRP1 repression for Snail-dependent transformation of HBECs *in vitro* and *in vivo*, it was hypothesized that pulmonary premalignant lesions observed in clinical biospecimens would also be characterized by ESRP1 silencing. Thus, pulmonary premalignant lesions previously identified as Snail-expressing were immunostained for ESRP1 (n=12). While ESRP1 is moderately-to-intensely expressed in tumor-adjacent histologically normal-appearing large and small airways, it is faint-to-absent in all premalignant lesions and tumor tissues examined (Fig 7K); isotype controls were negative (Figure S4A). These findings suggest that the Snail-ESRP1-cancer axis identified utilizing the HBEC lung cancer pathogenesis model may also be operative in human premalignancy *in situ*.

Discussion

While the mechanistic details and clinical implications of Snail-driven EMT occurring in advanced stage malignancy are partially resolved, the full impact of the EMT program on human cancer initiation and early progression remains to be determined. Here, we found that the transcription factor Snail is sufficient to malignantly transform normal and at-risk human bronchial epithelial cells via suppression of the epithelial splicing factor ESRP1. Because our previous studies indicate that EMT-inducing transcription factors may be up-regulated by inflammatory mediators richly present in the pulmonary microenvironment of patients at-risk for lung cancer (19), our current findings suggest that an inflammation-Snail-ESRP1 axis may collaborate with oncogenic mutational events to precipitate malignant

transformation and tumor progression *in situ*. Indeed, we found that pulmonary premalignant lesions from archived clinical specimens are characterized by inflammation and Snail expression concomitant with ESRP1 loss.

In preclinical studies, we previously documented Snail expression as a feature of established lung cancers with a proclivity to progress and metastasize (8,9). The current investigation utilizing *in vitro* and *in vivo* models of human lung carcinogenesis indicates that Snail also plays a significant role in tumor initiation, consistent with findings in murine models (2,20). The robustness of the contribution of Snail to lung carcinogenesis is underscored by the observation that Snail alone is sufficient to induce malignant transformation of all cell lines examined *in vitro*, although *P53* loss and *KRAS* activation are both necessary for tumor formation and metastatic behavior *in vivo*. Whereas other groups have identified KRAS as the most important facilitator of epithelial cell transformation in their *in vivo* model systems (6,21), P53 appears to fuel the Snail-driven transformation observed in the current study, consistent with the SCC histology of the xenograft tumors observed. A similar synergy between Snail and P53 has been described in other solid tumor models (2,22). The key contribution of KRAS to *in vivo* transformation in our model may be support of the stem cell phenotype, including direct suppression of stemness-repressing miRs, such as miR-200, -203, and -183 (23). Maintenance of the stem cell niche is likely important in this setting, given the nearly 60-day lag phase that precedes palpation of the Snail tumors *in vivo*.

Indeed, the *in vitro* and *in vivo* data presented here indicate that the stem cell signaling program may ultimately underlie the broad impact of Snail on premalignant cells and its culmination in epithelial transformation. In other model systems, Snail has been found to enhance the reprogramming of somatic cells to pluripotency (24), often occurring in part via repression of miRNAs that themselves regulate stem cell signaling (13). These previous reports are aligned with the current findings indicating a Snail-primed $ALDH^{+}CD44^{+}CD24^{-}$ cancer stem cell population is responsible for AIG *in vitro*, is retained in both Snail lung cancers and metastases *in vivo*, and is present in human premalignant lung lesions *in situ*. As has been reported in models of breast cancer and melanoma (25,26), Snail also drives oncogene and tumor suppressor gene dysregulation in pulmonary epithelial cells. Because these Snail-driven alterations occur against a background of enhanced stemness, their transformative impact is likely compounded.

Like Snail, the epithelial splicing factor ESRP1 is frequently cited for its regulation of EMT and stemness programs in models of established cancer (27–29). ESRP1 has also been linked to dysregulation of oncogenes and tumor suppressor genes (30) as well as to motility and metastatic colonization (17,18,31–33), phenotypes that also overlap with Snail expression. Indeed, Snail repression of ESRP1 is known to promote EMT and drive tumorigenesis in other model systems (3–5). The current study now expands the role of ESRP1 to include mediation of Snail-driven human lung carcinogenesis. Specifically, we determined that Snail-expressing HBECs have concomitantly repressed ESRP1, and ESRP1 was identified as a requirement for Snail-dependent transformation of HBECs *in vitro* and *in vivo*. The observation of ESRP1 silencing coincident with Snail expression in the earliest pulmonary carcinogenic events observed *in situ* suggests that ESRP1 may facilitate the malignant transformation of premalignant lesions *in situ*, as well as their simultaneous

micrometastatic dissemination to distant sites. Investigations of large panels of cancer cells and previously published clinical datasets identified a role for ESRP1 in epigenetic regulation of EMT events associated with aggressive lung cancer histology, tumor responsiveness, and resistance (34,35). While this previously published work points to the potential for ESRP1 as a biomarker or target in advanced stage NSCLC, our findings suggest that ESRP1 may also be relevant during early disease pathogenesis. Given their intimately linked regulatory roles in EMT, transformation, and migration, it is anticipated that many of the cancer-associated phenotypes currently attributed to Snail may ultimately be attributable to ESRP1 suppression mechanistically. The mechanism by which Snail and ESRP1 cooperate to facilitate malignant phenotypes, including Snail-induced carcinogenesis reported here and Snail-induced host immune suppression reported by Kudo-Saito (36), is the next important question to address.

In summary, we utilized the HBEC human lung carcinogenesis model for an isogenic investigation of normal human epithelial cells throughout their transition into fully malignant cells capable of tumor formation and metastatic behavior *in vivo*. The role of inflammation-inducible Snail in the transformation of normal and at-risk human bronchial epithelial cells requires suppression of the epithelial splicing factor ESRP1. Our findings confirm the connection between the Snail, EMT, and stem cell signaling programs and identify a targetable splicing factor as the underlying mechanism of action and their culmination in transformation. The inflammation-Snail-ESRP1 axis may provide opportunities to intervene in the premalignant-to-cancer continuum for the potential benefit of those at risk for lung cancer.

Supplementary Material

Refer to Web version on PubMed Central for supplementary material.

Acknowledgments

The authors acknowledge the following core facilities and core funding sources: The UCLA Translational Pathology Core Laboratory; The UCLA GenoSeq and Clinical Microarray Cores; The UCLA Jonsson Comprehensive Cancer Center (JCCC) and Center for AIDS Research Flow Cytometry Core, supported by the National Institutes of Health (NIH) (#CA-16042 and #AI-28697).

Financial Support: This research was supported in part by funding from the National Cancer Institute (NCI) (#T32-HL072752 to S.M. Dubinett, #U01-CA152751 to S.M. Dubinett, #U01-CA176284 to J.D. Minna, and #P50-CA70907 to J.D. Minna), Department of Defense (DOD) (#W81XWH-10-1-1006 and #W81XWH-13-1-0460, both to S.M. Dubinett), Department of Veteran Affairs (VA) (#5I01BX000359 and #2I01BX000359, both to S.M. Dubinett), University of California Tobacco-Related Disease Research Program (TRDRP) (#18FT-0060 and #20KT-0055, both to T.C. Walser), and Cancer Prevention and Research Institute of Texas (CPRIT) (#RP110708 to J.D. Minna).

References

1. Albini A, DeCensi A, Cavalli F, Costa A. Cancer Prevention and Interception: A New Era for Chemopreventive Approaches. Clin Cancer Res. 2016
2. Mani SA, Guo W, Liao MJ, Eaton EN, Ayyanan A, Zhou AY, et al. The epithelial-mesenchymal transition generates cells with properties of stem cells. Cell. 2008; 133:704–15. [PubMed: 18485877]

3. De Craene B, Berx G. Regulatory networks defining EMT during cancer initiation and progression. Nature reviews Cancer. 2013; 13:97–110. [PubMed: 23344542]
4. De Craene B, Denecker G, Vermassen P, Taminau J, Mauch C, Derore A, et al. Epidermal Snail expression drives skin cancer initiation and progression through enhanced cytoprotection, epidermal stem/progenitor cell expansion and enhanced metastatic potential. Cell Death Differ. 2014; 21:310–20. [PubMed: 24162662]
5. Reinke LM, Xu Y, Cheng C. Snail represses the splicing regulator epithelial splicing regulatory protein 1 to promote epithelial-mesenchymal transition. The Journal of biological chemistry. 2012; 287:36435–42. [PubMed: 22961986]
6. Sato M, Larsen JE, Lee W, Sun H, Shames DS, Dalvi MP, et al. Human lung epithelial cells progressed to malignancy through specific oncogenic manipulations. Mol Cancer Res. 2013; 11:638–50. [PubMed: 23449933]
7. Sato M, Vaughan MB, Girard L, Peyton M, Lee W, Shames DS, et al. Multiple oncogenic changes (K-RAS(V12), p53 knockdown, mutant EGFRs, p16 bypass, telomerase) are not sufficient to confer a full malignant phenotype on human bronchial epithelial cells. Cancer Res. 2006; 66:2116–28. [PubMed: 16489012]
8. Yanagawa J, Walser TC, Zhu LX, Hong L, Fishbein MC, Mah V, et al. Snail promotes CXCR2 ligand-dependent tumor progression in non-small cell lung carcinoma. Clinical Cancer Research. 2009; 15:6820–9. [PubMed: 19887480]
9. Grant JL, Fishbein MC, Hong LS, Krysan K, Minna JD, Shay JW, et al. A novel molecular pathway for Snail-dependent, SPARC-mediated invasion in non-small cell lung cancer pathogenesis. Cancer prevention research. 2014; 7:150–60. [PubMed: 24253315]
10. Rawlins EL, Okubo T, Xue Y, Brass DM, Auten RL, Hasegawa H, et al. The role of Scgb1a1+ Clara cells in the long-term maintenance and repair of lung airway, but not alveolar, epithelium. Cell stem cell. 2009; 4:525–34. [PubMed: 19497281]
11. Lee SH, Lee SJ, Jung YS, Xu Y, Kang HS, Ha NC, et al. Blocking of p53-Snail binding, promoted by oncogenic K-Ras, recovers p53 expression and function. Neoplasia. 2009; 11:22–31. 6p following. [PubMed: 19107228]
12. Shimono Y, Zabala M, Cho RW, Lobo N, Dalerba P, Qian D, et al. Downregulation of miRNA-200c links breast cancer stem cells with normal stem cells. Cell. 2009; 138:592–603. [PubMed: 19665978]
13. Wellner U, Schubert J, Burk UC, Schmalhofer O, Zhu F, Sonntag A, et al. The EMT-activator ZEB1 promotes tumorigenicity by repressing stemness-inhibiting microRNAs. Nature cell biology. 2009; 11:1487–95. [PubMed: 19935649]
14. Patel M, Lu L, Zander DS, Sreerama L, Coco D, Moreb JS. ALDH1A1 and ALDH3A1 expression in lung cancers: correlation with histologic type and potential precursors. Lung Cancer. 2008; 59:340–9. [PubMed: 17920722]
15. Shao C, Sullivan JP, Girard L, Augustyn A, Yenerall P, Rodriguez-Canales J, et al. Essential role of aldehyde dehydrogenase 1A3 for the maintenance of non-small cell lung cancer stem cells is associated with the STAT3 pathway. Clin Cancer Res. 2014; 20:4154–66. [PubMed: 24907115]
16. Kim CF, Jackson EL, Woolfenden AE, Lawrence S, Babar I, Vogel S, et al. Identification of bronchioalveolar stem cells in normal lung and lung cancer. Cell. 2005; 121:823–35. [PubMed: 15960971]
17. Ishii H, Saitoh M, Sakamoto K, Kondo T, Katoh R, Tanaka S, et al. Epithelial splicing regulatory proteins 1 (ESRP1) and 2 (ESRP2) suppress cancer cell motility via different mechanisms. The Journal of biological chemistry. 2014; 289:27386–99. [PubMed: 25143390]
18. Lu ZX, Huang Q, Park JW, Shen S, Lin L, Tokheim CJ, et al. Transcriptome-wide landscape of pre-mRNA alternative splicing associated with metastatic colonization. Mol Cancer Res. 2015; 13:305–18. [PubMed: 25274489]
19. Dohadwala M, Yang S-C, Luo J, Sharma S, Batra RK, Huang M, et al. Cyclooxygenase-2-dependent regulation of E-cadherin: prostaglandin E(2) induces transcriptional repressors ZEB1 and snail in non-small cell lung cancer. Cancer Research. 2006; 66:5338–45. [PubMed: 16707460]

20. Cho MH, Park JH, Choi HJ, Park MK, Won HY, Park YJ, et al. DOT1L cooperates with the c-Myc-p300 complex to epigenetically derepress CDH1 transcription factors in breast cancer progression. Nat Commun. 2015; 6:7821. [PubMed: 26199140]
21. Larsen JE, Nathan V, Osborne JK, Farrow RK, Deb D, Sullivan JP, et al. ZEB1 drives epithelial-to-mesenchymal transition in lung cancer. J Clin Invest. 2016
22. Cho JH, Lee SJ, Oh AY, Yoon MH, Woo TG, Park BJ. NF2 blocks Snail-mediated p53 suppression in mesothelioma. Oncotarget. 2015; 6:10073–85. [PubMed: 25823924]
23. Zhong X, Zheng L, Shen J, Zhang D, Xiong M, Zhang Y, et al. Suppression of mir-200 family expression by oncogenic KRAS activation promotes cell survival and epithelial-mesenchymal transition in KRAS-driven cancer. Mol Cell Biol. 2016
24. Unternaehrer JJ, Zhao R, Kim K, Cesana M, Powers JT, Ratanasirintrawoot S, et al. The epithelial-mesenchymal transition factor SNAIL paradoxically enhances reprogramming. Stem cell reports. 2014; 3:691–8. [PubMed: 25316190]
25. Massoumi R, Kuphal S, Hellerbrand C, Haas B, Wild P, Spruss T, et al. Down-regulation of CYLD expression by Snail promotes tumor progression in malignant melanoma. J Exp Med. 2009; 206:221–32. [PubMed: 19124656]
26. Mitra S, Federico L, Zhao W, Dennison J, Sarkar TR, Zhang F, et al. Rab25 acts as an oncogene in luminal B breast cancer and is causally associated with Snail driven EMT. Oncotarget. 2016
27. Barbachano A, Fernandez-Barral A, Pereira F, Segura MF, Ordonez-Moran P, Carrillo-de Santa Pau E, et al. SPROUTY-2 represses the epithelial phenotype of colon carcinoma cells via upregulation of ZEB1 mediated by ETS1 and miR-200/miR-150. Oncogene. 2016; 35:2991–3003. [PubMed: 26455323]
28. Fagoonee S, Bearzi C, Di Cunto F, Clohessy JG, Rizzi R, Reschke M, et al. The RNA binding protein ESRP1 fine-tunes the expression of pluripotency-related factors in mouse embryonic stem cells. PloS one. 2013; 8:e72300. [PubMed: 24015231]
29. Voena C, Varesio LM, Zhang L, Menotti M, Poggio T, Panizza E, et al. Oncogenic ALK regulates EMT in non-small cell lung carcinoma through repression of the epithelial splicing regulatory protein 1. Oncotarget. 2016
30. Zhu X, Asa SL, Ezzat S. Genetic and epigenetic mechanisms down-regulate FGF receptor 2 to induce melanoma-associated antigen A in breast cancer. Am J Pathol. 2010; 176:2333–43. [PubMed: 20348248]
31. Lu H, Liu J, Liu S, Zeng J, Ding D, Carstens RP, et al. Exo70 isoform switching upon epithelial-mesenchymal transition mediates cancer cell invasion. Developmental cell. 2013; 27:560–73. [PubMed: 24331928]
32. Yae T, Tsuchihashi K, Ishimoto T, Motohara T, Yoshikawa M, Yoshida GJ, et al. Alternative splicing of CD44 mRNA by ESRP1 enhances lung colonization of metastatic cancer cell. Nat Commun. 2012; 3:883. [PubMed: 22673910]
33. Di Modugno F, Iapicca P, Boudreau A, Mottolese M, Terrenato I, Perracchio L, et al. Splicing program of human MENA produces a previously undescribed isoform associated with invasive, mesenchymal-like breast tumors. Proceedings of the National Academy of Sciences of the United States of America. 2012; 109:19280–5. [PubMed: 23129656]
34. Kohn KW, Zeeberg BM, Reinhold WC, Pommier Y. Gene expression correlations in human cancer cell lines define molecular interaction networks for epithelial phenotype. PloS one. 2014; 9:e99269. [PubMed: 24940735]
35. Lin SH, Wang J, Saintigny P, Wu CC, Giri U, Zhang J, et al. Genes suppressed by DNA methylation in non-small cell lung cancer reveal the epigenetics of epithelial-mesenchymal transition. BMC genomics. 2014; 15:1079. [PubMed: 25486910]
36. Kudo-Saito C, Shirako H, Takeuchi T, Kawakami Y. Cancer metastasis is accelerated through immunosuppression during Snail-induced EMT of cancer cells. Cancer Cell. 2009; 15:195–206. [PubMed: 19249678]

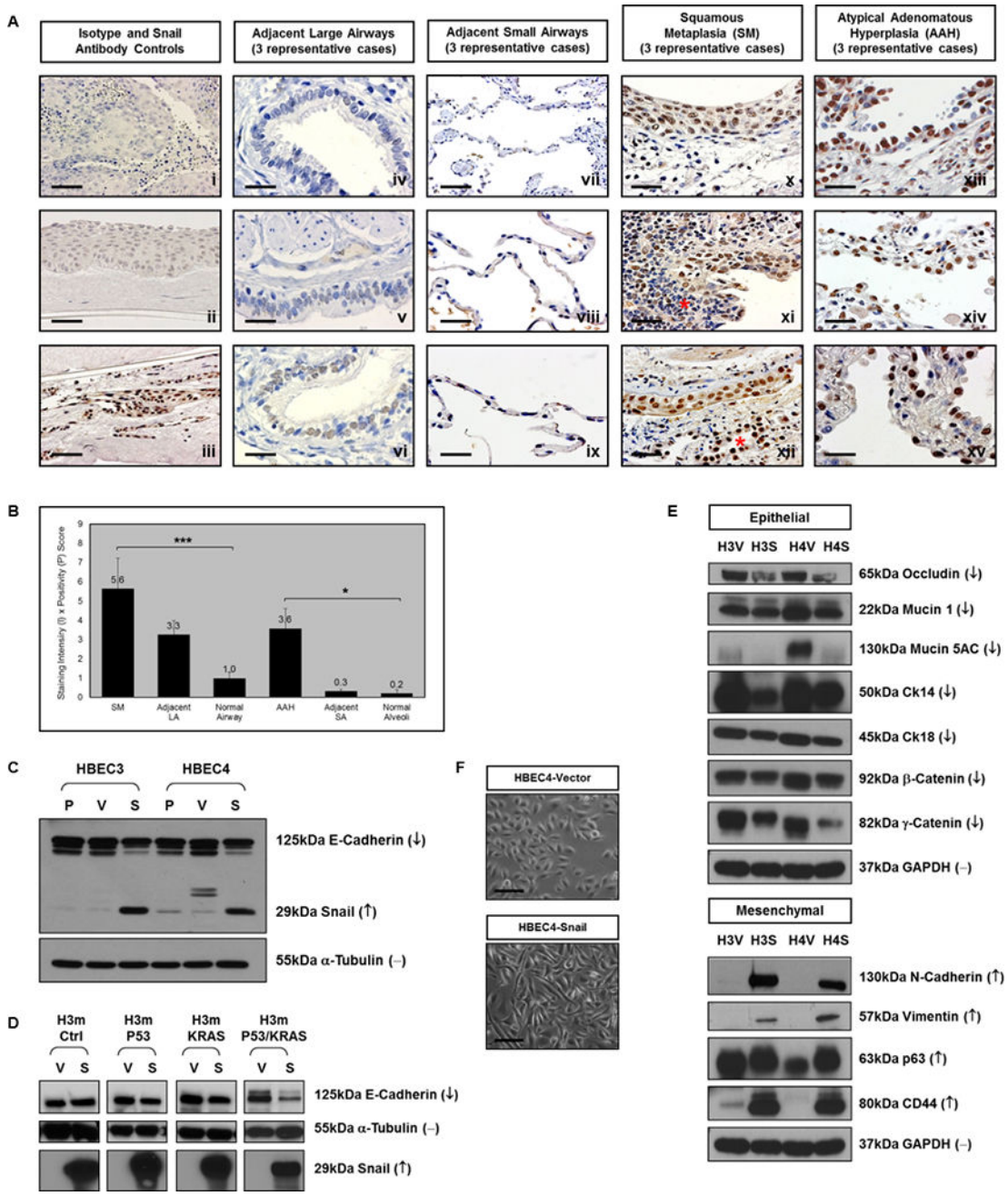

Figure 1. Snail expression is observed in human pulmonary premalignant lesions and drives EMT in an HBEC-based model of lung premalignancy

Representative fields at 400X; scale bar = 50 μm. (**A**) (**i**) Isotype control staining of a NSCLC tumor previously identified as Snail-positive (11). Snail staining of (**ii**) HBEC-Vector cells (negative control) and (**iii**) HBEC-Snail cells (positive control) grown in 3D ALI culture. Snail staining of (**iv-vi**) SCC-adjacent LAs and (**vii-ix**) ADC-adjacent SAs. Snail staining of (**x-xii**) SM premalignant lesions, where **xi-asterisk** denotes a representative focus of inflammation and **xii-asterisk** denotes a representative field of hyperplasia. Snail staining of (**xiii-xv**) AAH premalignant lesions. (**B**) Snail immunostaining was quantitated by

assigning Intensity (I) and Positivity (P) scores (each on a scale from 0 to 4, low to high) and calculating IxP values. (**C**) Normal HBEC-Parental (P), -Vector (V), and -Snail (S) were evaluated for Snail and E-Cadherin expression by Western Blot (WB) analysis. (**D**) At-risk oncogene-modified HBEC-V and -S were evaluated for Snail and E-Cadherin. Normal HBEC-V and -S were (**E**) probed for a panel of epithelial and mesenchymal markers of the EMT program and (**F**) evaluated for morphology indicative of EMT; **top** = cobblestone epithelial morphology, and **bottom** = spindle-shaped mesenchymal morphology.

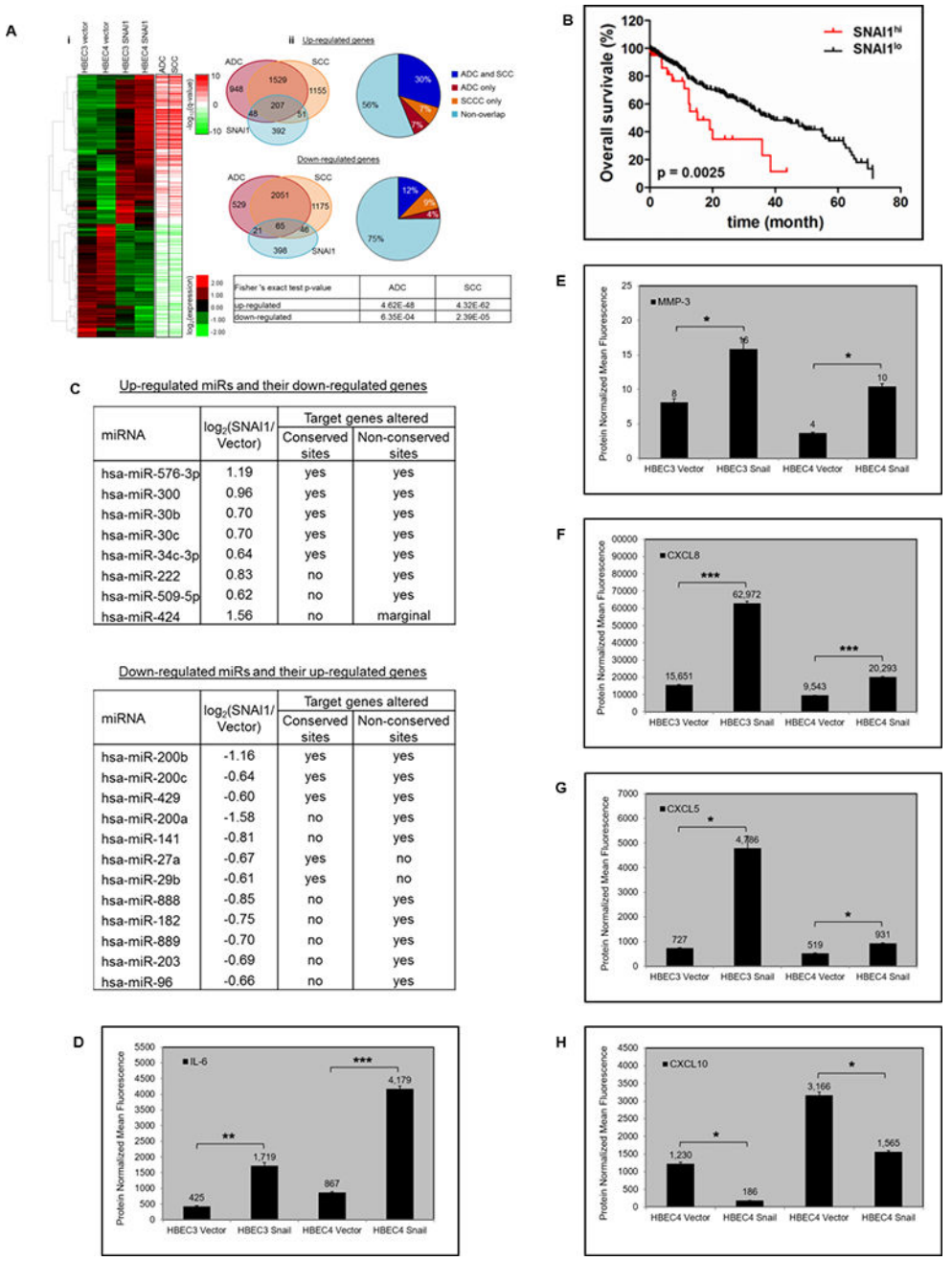

Figure 2. Genomic and proteomic profiling reveal Snail-driven cancer-associated signaling nodes operative during pulmonary premalignancy

(**A**) Differential gene expression was evaluated using Affymetrix U133 Plus 2.0 gene arrays and bioinformatic analyses. (**i- four left columns**) A heatmap of differential gene expression (> 2 FC). (**i- two right columns**) Color-coded log10-transformed q-values of (**red**) up- and (**green**) down-regulated genes observed in human NSCLC tumors relative to normal lung tissue. (**ii- venn diagrams and pie charts**) Summary of overlap between Snail-dependent genes identified in the HBEC-Snail dataset and dysregulated genes observed in previously published clinical lung cancer datasets. (**ii- table**) Summary of fisher exact tests justifying

the reported overlap. (**B**) Survival analysis of Snail within the lung SCC TCGA dataset. (**C**) Differential miRNA expression was evaluated using Exiqon miRCURY microRNA arrays and bioinformatic analyses. Fisher exact tests were used to determine if statistically significant ($p < 0.05$) overlap occurred between target genes of a miRNA and differentially expressed genes. (**D-H**) Luminex multiplex assays were used to measure secreted proteins IL-6, MMP-3, CXCL8, CXCL5, and CXCL10.

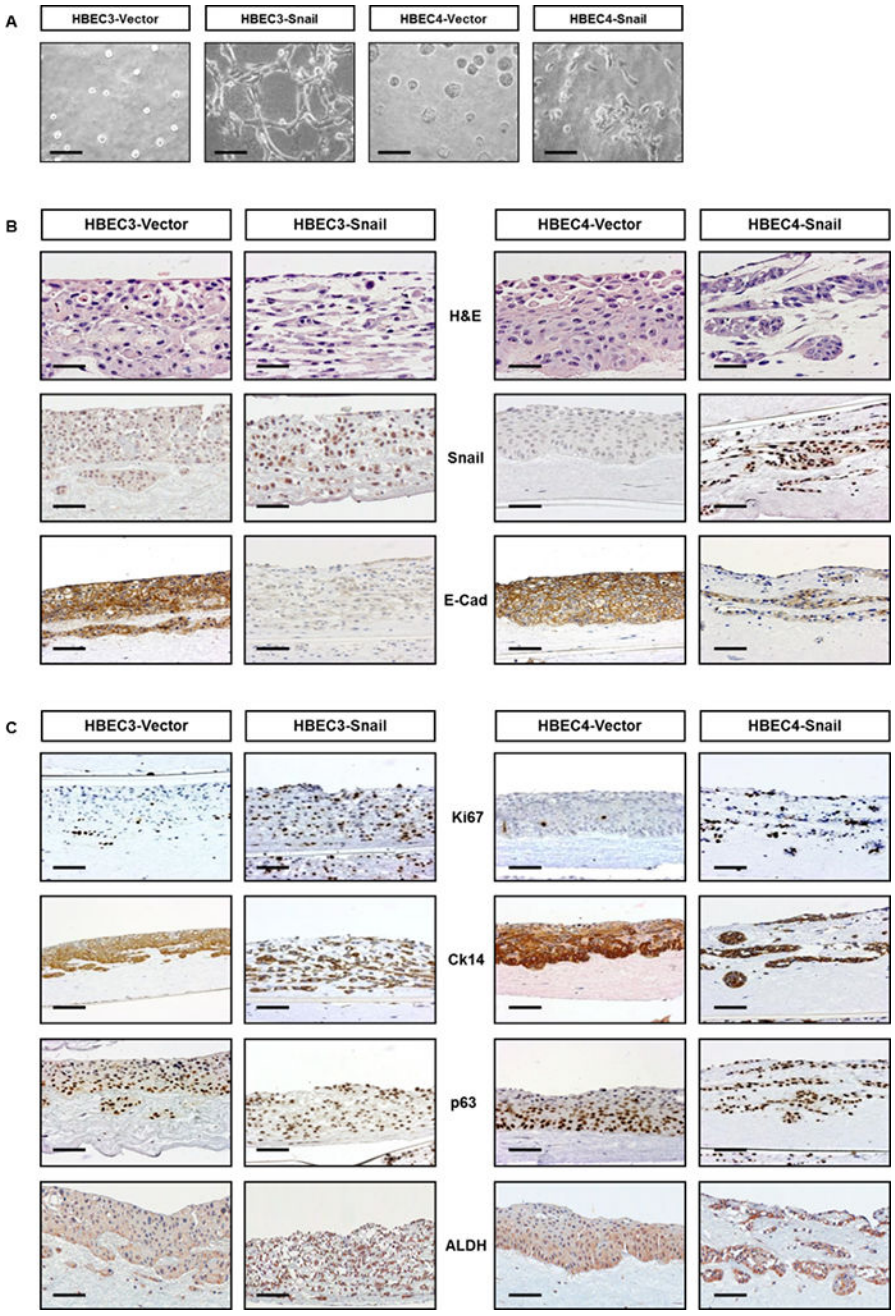

Figure 3. Snail drives key malignant phenotypes in 3D models of lung carcinogenesis

(**A**) Normal HBEC-V and -S were cultured in a 3D spheroid model and evaluated for morphology indicative of EMT and invasion; representative 400X fields at d3 of growth. (**B-C**) HBEC-Vector and -Snail were cultured in a 3D lung organotypic ALI model; representative 400X fields at d14 of growth. (**B**) The cultures were H&E stained and immunostained for Snail and E-Cadherin to assess EMT and invasion. (**C**) They were immunostained for markers of proliferation (Ki67), differentiation (Ck14 and p63), and stemness (Ck14, p63, and ALDH).

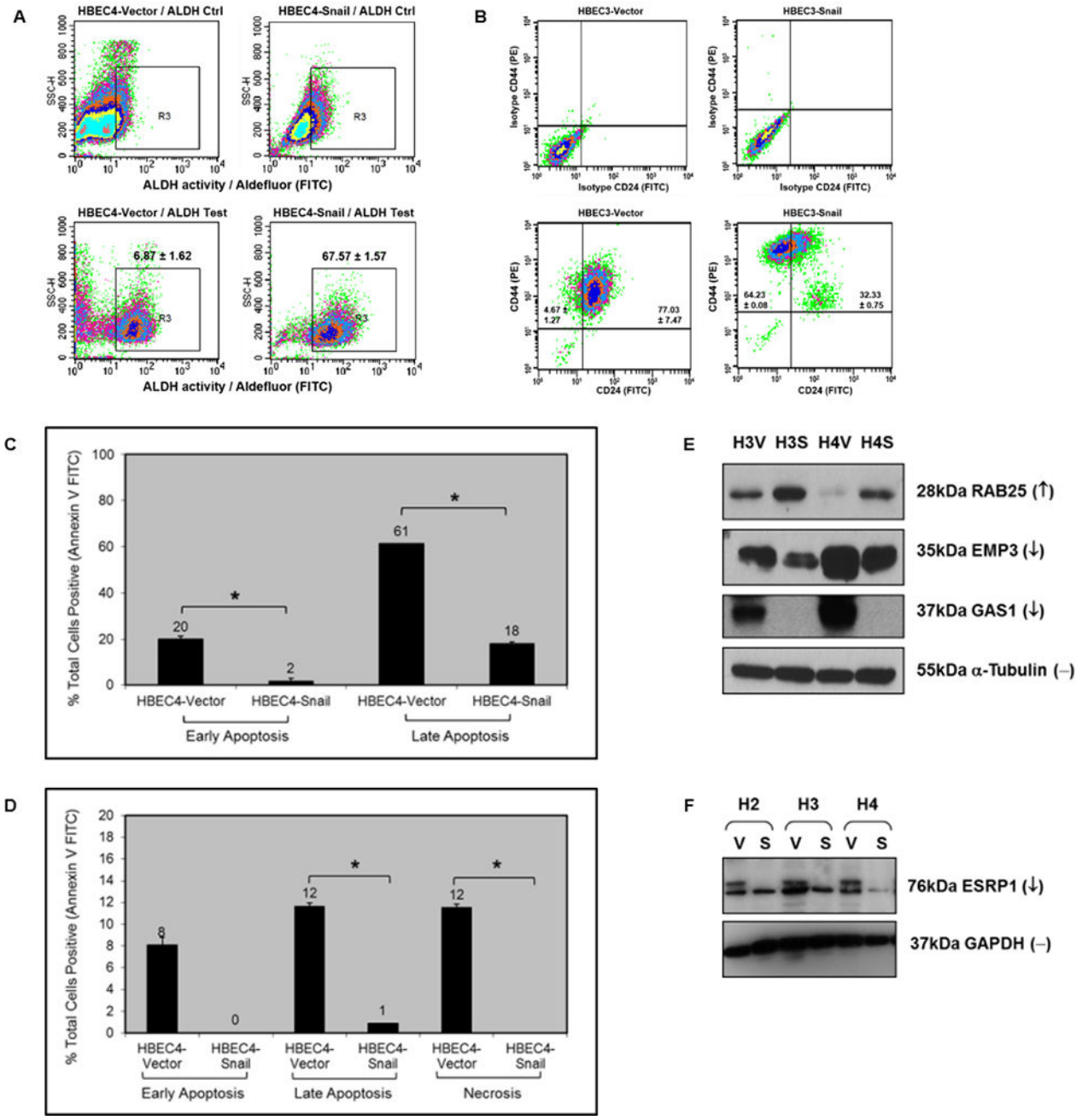

Figure 4. Snail drives stemness expansion, apoptosis resistance, and dysregulation of oncogene and tumor suppressor gene expression

(**A**) ALDH activity levels and (**B**) the $CD44^{+}CD24^{-}$ cancer stem cell phenotype were evaluated in HBEC-Vector and -Snail via flow cytometry. (**C-D**) HBEC-Vector versus -Snail susceptibility to apoptosis in response to two distinct stimuli was assessed via flow cytometry; LR = early apoptosis, UR = late apoptosis, and UL = necrosis. (**E-F**) The expression patterns of select oncogenes (RAB25) and tumor suppressors (EMP3, GAS1, and ESRP1) were surveyed by WB analysis.

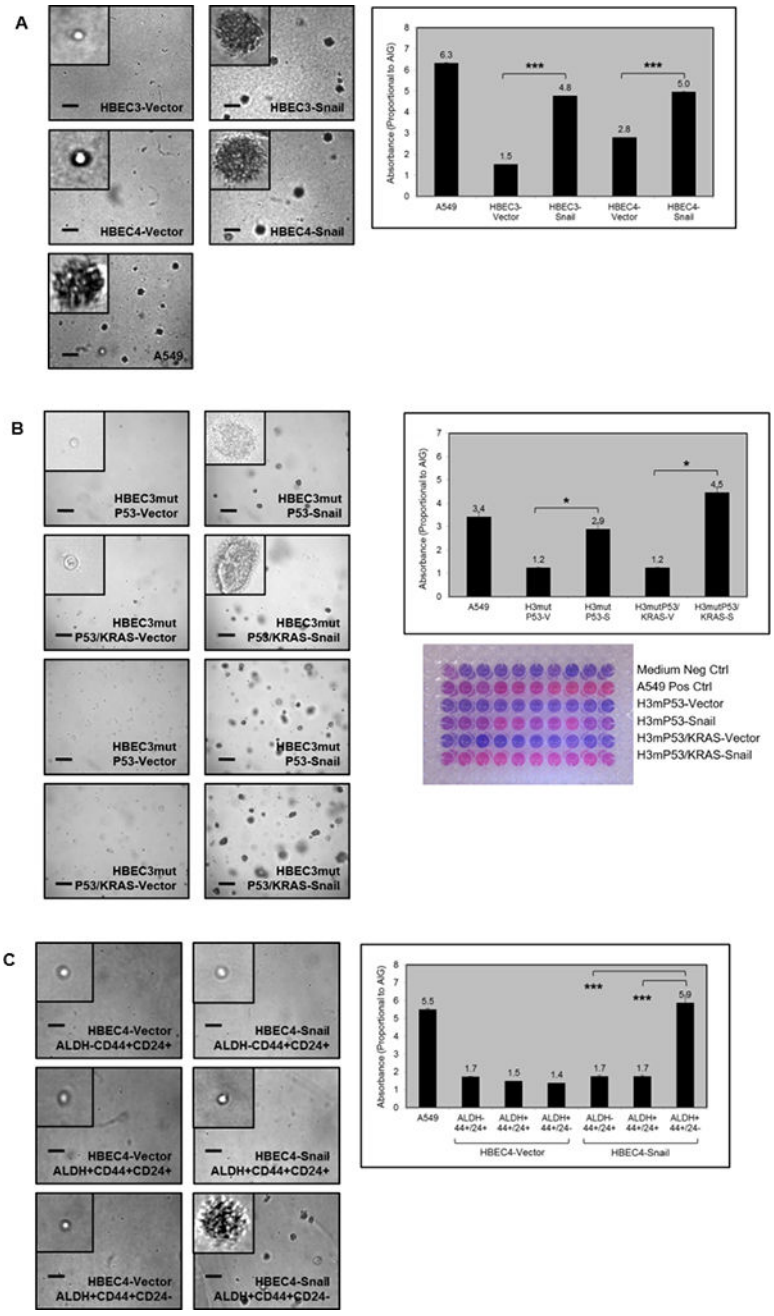

Figure 5. Snail-driven malignant transformation is augmented by driver mutations and is dependent on acquisition of stem-like traits

(**A**) The capacity of normal HBEC-V and -S for AIG was evaluated by seeding the cells in a miniaturized AIG assay; 1000 cells per well of a 96 well plate with 8 replicates per condition. After 2 weeks in culture, colonies were assessed by (**photos**) gross microscopic examination and (**bar graph**) biochemical assay. Each field is 20X, and each inset is 40X and centered on a representative colony in the same well. Absorbance was detected at 570 nm (600 nm reference) and is directly proportional to AIG. (**B**) HBEC3-V and -S harboring P53 loss (H3mP53) or the combination of P53 loss and KRAS activation (H3mP53/KRAS)

were evaluated for AIG after 15 days in culture. (**C**) Three flow-sorted stem cell subsets, ALDH-CD44+CD24+, ALDH+CD44+CD24+, and ALDH+CD44+CD24-, evaluated for AIG after 15 days in culture.

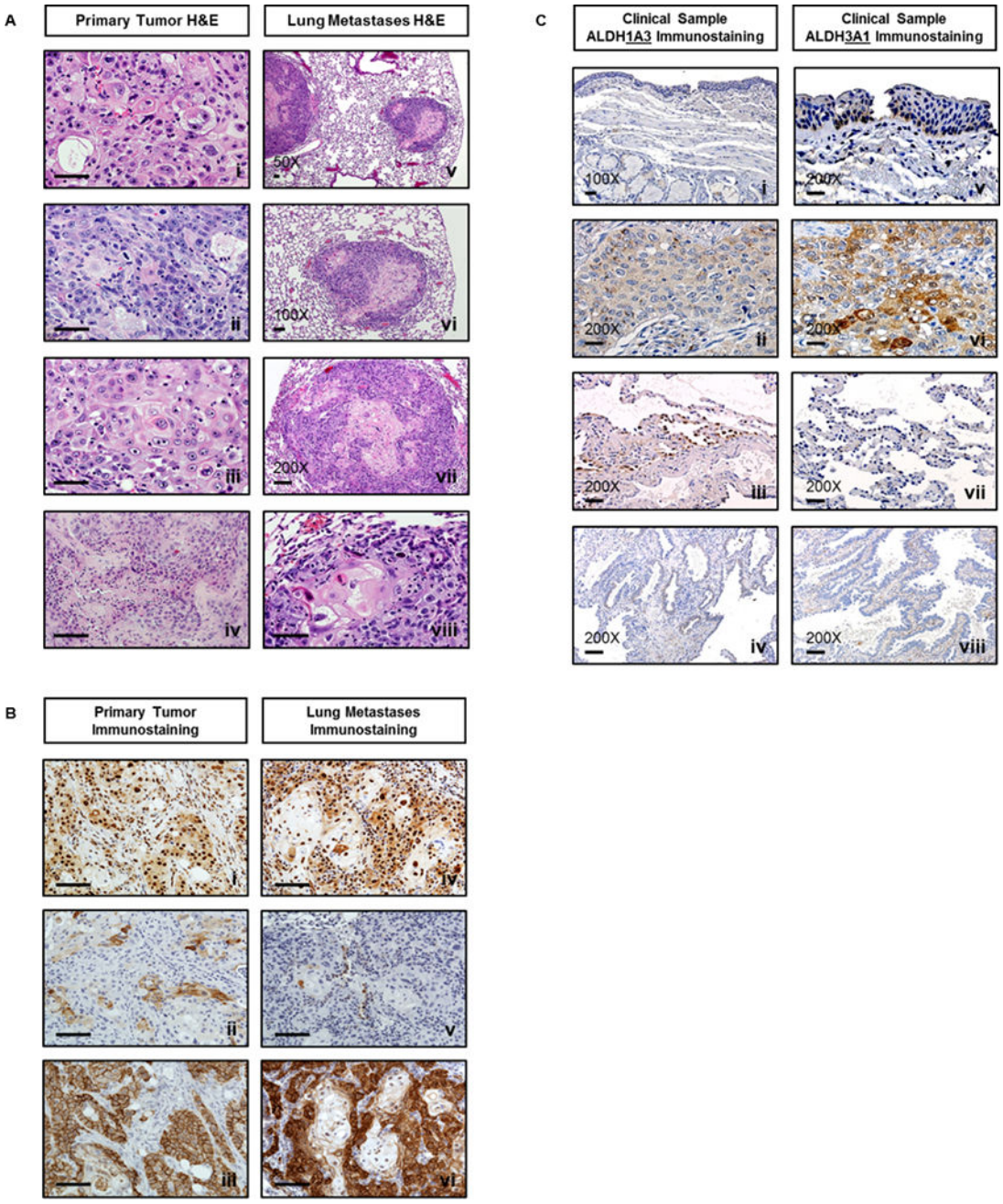

Figure 6. Snail drives malignant transformation, tumor growth, and metastasis of HBECs *in vivo*

Representative fields at 400X; scale bar = 50 μm. (**A-B**) H&E and IHC evaluation of primary tumors and lung metastases arising from H3mP53/KRAS-Snail cells injected SC in NSG mice. (**i-iv**) Four primary tumors representing each of the histologies observed are shown. (**v-viii**) Four fields depicting the pulmonary metastatic lesion number and size. Large and well-circumscribed nodules with keratin pearls and intracellular bridges indicative of SCC tumor histology were observed in every case. (**B**) H3mP53/KRAS-Snail cells transformed into primary tumors and lung metastases in mice were immunostained for (**top row**) Snail, (**middle row**) ALDH, and (**bottom row**) CD44, all of which were required for

tumor-initiating capacity *in vitro*. (**C**) Human clinical specimens containing SM-SCC or AAH-AIS-ADC were immunostained for ALDH1A3 and ALDH3A1.

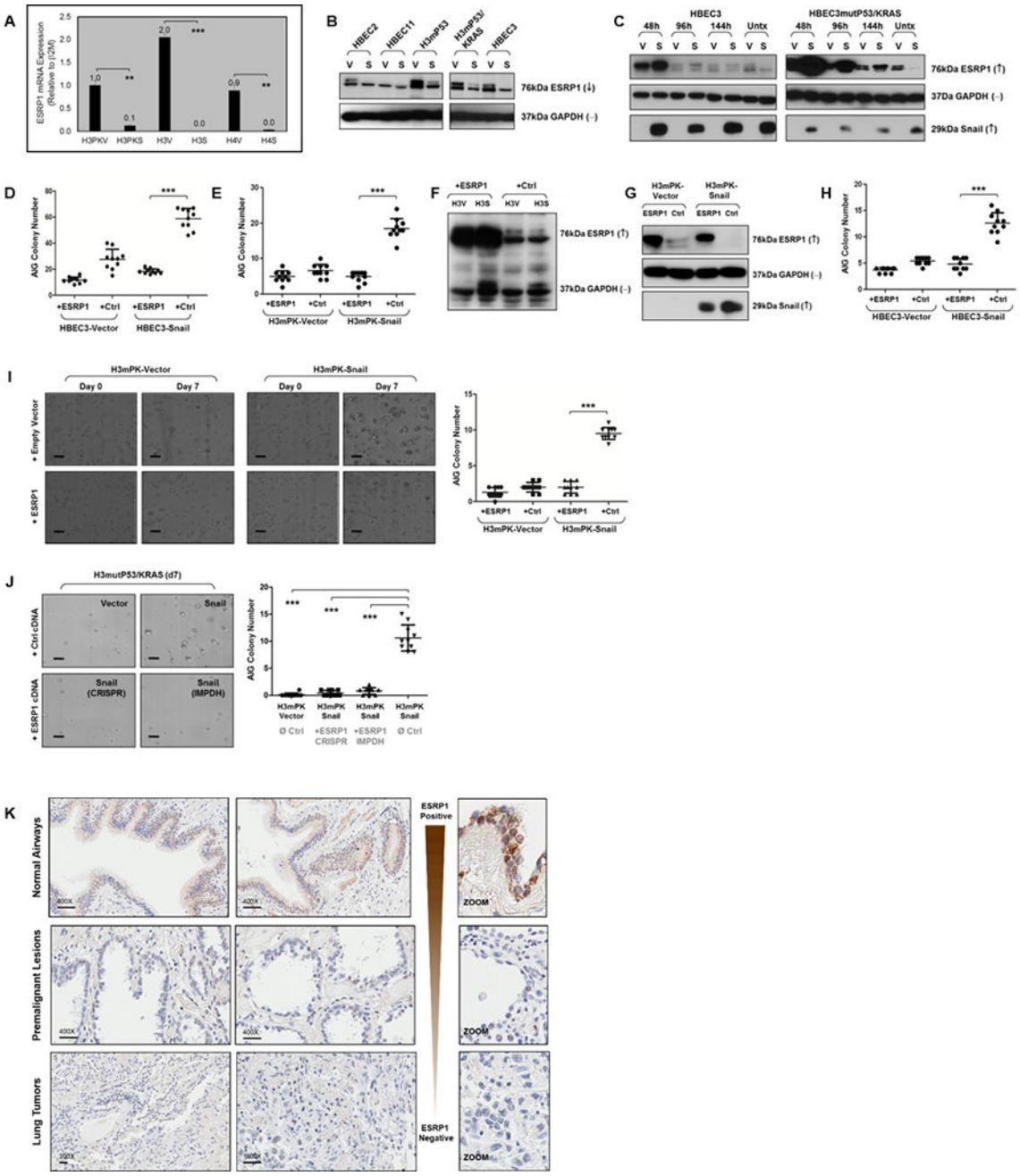

Figure 7. Snail-dependent ESRP1 silencing drives human pulmonary epithelial cell transformation

(**A**) Basal expression of ESRP1 was measured by qRT-PCR and normalized to B2M. (**B**) WB analysis performed for Snail, ESRP1, and housekeeping gene expression. (**C**) WB analysis performed for Snail, ESRP1, and GAPDH expression in HBEC3-V and -S and H3mutP53/KRAS-V and -S transiently transfected with ESRP1-specific cDNA constructs (and untreated control cells). (**D**) Normal HBEC3-V and -S with transient re-expression of ESRP1 were seeded in an accelerated AIG assay at 3000K cells/well with 10 replicates. Z-stacked photomicrographs of each well were created on d0 and d5. Each dot on the graph

represents the number of colonies counted from each 3D focused image of each well. (**E**) At-risk HBEC3-P53/KRAS-V and -S with transient re-expression of ESRP1 were seeded in an AIG assay. (**F**) Normal and (**G**) at-risk HBEC-S with stable re-expression of ESRP1 were evaluated for Snail and ESRP1 expression by WB analysis. The (**H**) normal and (**I**) at-risk HBEC-S were then then seeded in an AIG assay and assessed after 7 days of growth. (**J**) Transduction with ESRP1 or control cDNA was repeated using two different approaches (CRISPR method with Hygromycin B selection or IMPDH method with MPA selection), before the normal and at-risk cells were evaluated for Snail and ESRP1 expression by WB analysis and seeded in an AIG assay. (**K**) Pulmonary premalignant lesions with high level Snail expression in Figure 1 (n=12) were evaluated for ESRP1 expression. Representative fields at 400X; scale bar = 50 μm.